

1

2 **Evidence of solid Earth influence on stability of the marine-terminating Puget**  
3 **Lobe of the Cordilleran Ice Sheet**

3

4 **Marion A. McKenzie<sup>1\*</sup>, Lauren E. Miller<sup>1</sup>, Allison P. Lepp<sup>1</sup>, and Regina DeWitt<sup>2</sup>**

5 <sup>1</sup>Department of Environmental Sciences, University of Virginia, 291 McCormick Rd.,  
6 Charlottesville, VA, USA 22904 <sup>2</sup>Department of Physics, East Carolina University, 1000  
7 E. 5<sup>th</sup> St., Greenville, NC, USA 27858-4353

8 Corresponding author: Marion McKenzie ([marion.mckenzie@mines.edu](mailto:marion.mckenzie@mines.edu))

9 \* Author now affiliated with the Geology and Geological Engineering Department,  
10 Colorado School of Mines, 1105 Illinois St., Golden, CO, USA 80201

11 **Key Points:**

- 12 • Solid Earth uplift is capable of stabilizing marine-terminating ice streams and  
13 seen in stratigraphy across the Puget Lowland.
- 14 • The Puget Lobe of the Cordilleran Ice Sheet was present in the Puget Lowland  
15 until at least 12,100 calendar years before present.
- 16 • A newly developed marine reservoir for the Puget Lowland is found to be 264 <sup>14</sup>C  
17 years or 50 calendar years before present.  
18

## 19 **Abstract**

20 Understanding drivers of marine-terminating ice sheet behavior is important for constraining ice  
21 contributions to global sea-level rise. In part, the stability of marine-terminating ice is influenced  
22 by solid-Earth conditions at the grounded-ice margin. While the Cordilleran Ice Sheet (CIS)  
23 contributed significantly to global mean sea level during its final post-Last Glacial Maximum  
24 (LGM) collapse, the drivers and patterns of retreat are not well constrained. Coastal outcrops in  
25 the deglaciated Puget Lowland of Washington state - largely below sea level during glacial  
26 maxima, then uplifted above sea level via glacial isostatic adjustment (GIA) - record late  
27 Pleistocene history of the CIS. The preservation of LGM glacial and post-LGM deglacial  
28 sediments provides a unique opportunity to assess variability in marine ice-sheet behavior of the  
29 southernmost CIS. Based on paired stratigraphic and geochronological work with a newly  
30 developed marine-reservoir correction for this region, we identify that the late-stage CIS  
31 experienced stepwise retreat into a marine environment about 12,000 years before present,  
32 placing glacial ice in the region for about 3,000 years longer than previously thought. Stand-still  
33 of marine-terminating ice for a millenia, paired with rapid vertical landscape evolution, was  
34 followed by continued retreat of ice in a subaerial environment. These results suggest rapid rates  
35 of solid Earth uplift and topographic support (e.g., grounding-zone wedges) stabilized the ice-  
36 margin, supporting final subaerial ice retreat. This work leads to a better understanding of shallow  
37 marine and coastal ice sheet retreat; relevant to sectors of the contemporary Antarctic and  
38 Greenland ice sheets and marine-terminating outlet glaciers.

## 39 **Plain Language Summary**

40 Glaciers that deposit ice directly into the ocean are capable of losing large amounts of ice  
41 that contribute to global sea level rise. The surface that glaciers sit on can influence how  
42 quickly ice is lost to the ocean. Vertical movement of solid Earth, as a result of large ice  
43 losses, is capable of stopping glacial retreat in an ocean environment. Records of the  
44 interaction between Earth and glacial ice movement are contained in the sediments along  
45 the coast of the Puget Lowland in Washington state. This work finds that glacial ice in  
46 the Puget Lowland, from 20,000 years ago, was present in the area about 3,000 years  
47 longer than previously thought. We also interpret that solid Earth movement provided  
48 stability to this marine-terminating glacial ice for about 1,000 years. These results are  
49 significant because this landscape is similar to parts of the Greenland Ice Sheet and the  
50 Antarctic Peninsula, indicating that the interactions seen in this area are applicable to  
51 modern glaciated regions.

## 52 **1 Introduction**

53 The terrain and substrate geology beneath ice sheets have the potential to affect  
54 the behavior of the overriding ice; they can influence ice flow organization, velocity, and  
55 margin positions (Weertman, 1974; Clarke et al., 1977; Clark, 1994; Whillans & van der  
56 Veen, 1997; Cuffey & Paterson, 2010; Jamieson et al., 2012; Margold et al., 2015).  
57 Coupled ice sheet and solid Earth models indicate that glacial isostatic adjustment (GIA)  
58 can stabilize marine-based grounding lines (van der Wal et al., 2015; Whitehouse et al.,  
59 2019; Wan et al., 2022) but this relationship has yet to be tested empirically. Due to the  
60 difficulty in observing subglacial conditions and solid Earth dynamics beneath modern  
61 ice sheets, we turn to the deglacial sediment record of the extinct Cordilleran Ice Sheet  
62 (CIS) in the Puget Lowland. Specifically, we consider the marine-based southernmost

63 part of the CIS, the Puget Lobe, which most recently advanced across the Puget Lowland  
64 during the Last Glacial Maximum (~20,000 years ago; Mullineaux et al., 1965;  
65 Easterbrook et al., 1967; Easterbrook, 1969; Porter & Swanson, 1998). The Puget  
66 Lowland records vertical land change due to tectonics and glacial isostatic adjustment  
67 (GIA) from Puget Lobe advance and retreat in the region, making it an ideal location to  
68 study influence of solid Earth on ice-sheet behavior and post-glacial landscape evolution.  
69 Topographic similarities between the Puget Lowland and Greenland indicate the  
70 deglacial history of the Puget Lobe may be an appropriate analog for studying  
71 contemporary Greenland Ice Sheet outlet glaciers (Eyles et al., 2018). Additionally, the  
72 ice histories and solid Earth properties, such as flexural thickness of the lithosphere and  
73 mantle viscosity, in this region are similar to that of the Antarctic Peninsula (Nield et al.,  
74 2014; Whitehouse et al., 2019). Contributing to understanding the role of topography and  
75 solid-Earth conditions on marine-based glacial ice can lead to development of a process-  
76 based model on marine-terminating retreat of modern ice sheets. The findings from this  
77 work are relevant to modern glacial systems and have implications for timing of CIS  
78 contribution to global sea level as well as routes and timing of human migration into the  
79 Americas (Mandryk et al., 2001; Goebel et al., 2011; Lesnek et al., 2018).

80

### 81 **1.1 Regional Context**

82 The Puget Lowland of Washington state has been glaciated at least six times  
83 throughout the Quaternary as a result of CIS advance and retreat in the region.  
84 Glaciations occurred during marine isotope stage (MIS) 6 (~97,000 to 150,000 years ago;  
85 Easterbrook, 1969), MIS 4 (80,000 ± 20,000 years; Easterbrook et al., 1967; Easterbrook,  
86 1969), and towards the end of MIS 2 (~17,500 cal. year BP; Mullineaux et al., 1965;  
87 Porter & Swanson, 1998). Existing geochronology places final deglaciation of the Puget  
88 Lowland around 16,500 calendar years before present (cal. yr. B.P.) (Easterbrook, 1992;  
89 Dethier et al., 1995; Swanson & Caffee, 2001). Yet, the lack of detailed stratigraphic  
90 context for age constraints and absence of a local marine reservoir correction (MRC)  
91 have left uncertainties in the exact timing of ice retreat. Nonetheless, based on similarities  
92 in previously published radiometric ages, it is suggested that marine incursion drove  
93 rapid lift-off and northward retreat of the Puget Lobe (Thorson, 1980, 1981; Waitt and  
94 Thorson, 1983; Booth, 1987; Booth et al., 2003). However, there are variable records of  
95 deglacial stratigraphy across the region (Powell, 1980; Pessl et al., 1981; Domack, 1984;  
96 Demet et al., 2019), and the presence of ice-marginal landforms indicate periodic stand-  
97 still in ice margin during retreat (Simkins et al., 2017; Demet et al., 2019). Subsequently,  
98 the need to clarify spatiotemporal details of ice retreat patterns and drivers of Puget Lobe  
99 retreat persists.

100 The magnitude of landscape emergence due to GIA in the Puget Lowland may  
101 have been as high as 10 cm a<sup>-1</sup> during early deglaciation (Dethier et al., 1995), likely due  
102 to the elastic solid-Earth response to unloading (c.f. Whitehouse, 2018). This rate of GIA-

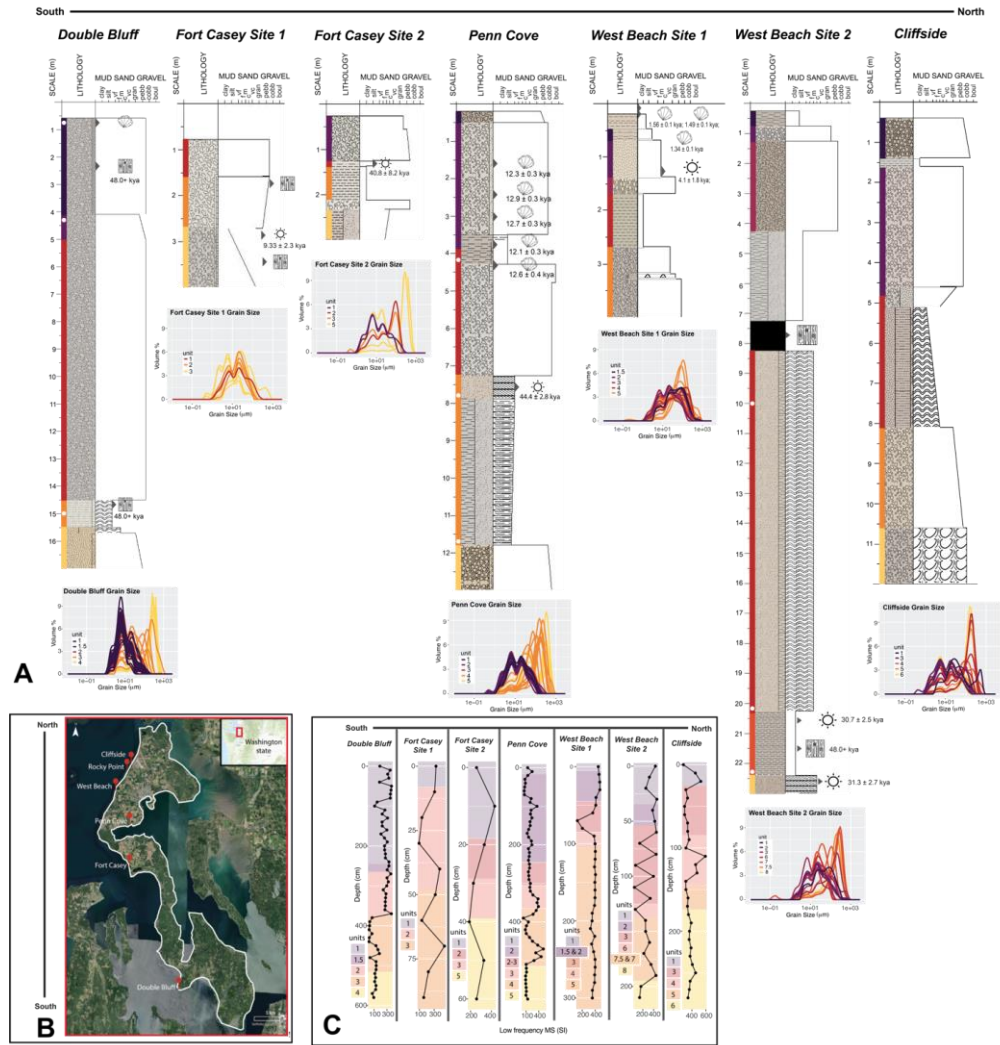
103 induced uplift suggests relative sea-level fall in the Puget Lowland outpaced rapid global  
104 sea-level rise, leading to emergence of the landscape from below to above sea level  
105 during the end of the LGM (Shugar et al., 2014; Yokoyama & Purcell, 2021). Both pre-  
106 existing topography and GIA could have periodically stabilized the Puget Lobe during  
107 retreat, as suggested for contemporary ice sheets (Durand et al., 2011; Favier et al., 2016;  
108 Alley et al., 2021; Robel et al., 2022), highlighting the importance of elucidating the role  
109 of both conditions on ice-sheet behavior.

110

## 111 **1.2 Relevance to solid Earth dynamics and modern ice sheets and glaciers**

112 Based on modelled evidence of GIA control on ice behavior in analogous  
113 Antarctic Peninsula glacial catchments (Nield et al., 2014; Whitehouse et al., 2019), in  
114 addition to previously identified geomorphic evidence of ice-margin stand still in the  
115 Puget Lowland (Simkins et al., 2017; Demet et al., 2019), we hypothesize that landscape  
116 position above and below sea level, due to loading and unloading of the solid Earth,  
117 influenced ice-margin positions and led to punctuated retreat of the CIS during the late  
118 Pleistocene. In the central Puget Lowland, Whidbey Island spans nearly 100 kilometers in  
119 distance along the North-South direction of glacial ice movement and hosts extensive  
120 coastal bluff features (Figure 1B). The outcrops, composed of glacial and interglacial  
121 sediments, preserve details of ice advance and retreat across the formerly marine  
122 landscape, as well as landscape transitions that took place coeval with deglaciation.  
123 Except for localized tectonic deformation of surficial sediments (Sherrod et al., 2008),  
124 local LGM and subsequent deglacial deposits appear to have little post-depositional  
125 reworking (Booth & Hallet, 1993; Kovanen & Slaymaker, 2004; Eyles et al., 2018;  
126 Demet et al., 2019; McKenzie et al., 2023).

127 In this work, decimeter-scale stratigraphic and sedimentological assessments are  
128 complemented by accelerator mass spectrometry radiocarbon ( $^{14}\text{C}$ ) and optically  
129 stimulated luminescence (OSL) dating. While these two dating methods have been  
130 utilized in this region for decades (e.g., Rigg and Gould, 1957; Leopold et al., 1982;  
131 Easterbrook, 1992; Anundsen et al., 1994; Dethier et al., 1995; Swanson and Caffee,  
132 2001), our hypothesis of the relationship and timing of landscape emergence in relation to  
133 ice retreat and periodic stabilization of ice retreat has not been directly assessed.  
134 Therefore, the application of advances in geochronology paired with a high-resolution  
135 stratigraphic assessment of Whidbey Island is a novel approach to elucidating the ice  
136 retreat and land emergence across the region.



137  
 138 **Figure 1.** A) Outcrop sites from south to north: Double Bluff, Fort Casey 1, Fort Casey 2,  
 139 Penn Cove, West Beach Site 1, West Beach Site 2, and Cliffside represented by  
 140 stratigraphic column with collected radiocarbon and OSL and grain size data below.  
 141 Colors alongside stratigraphic units indicate grain size measurement correlations. White  
 142 dots indicate changes to site collection of samples. B) Regional inset map with sites  
 143 labelled south to north . C) Magnetic susceptibility values for each site, listed south to  
 144 north, and colored boxes indicate stratigraphic unit correlations to values.  
 145

### 1.3 Contextualization of Outcrop Research in the Puget Lowland

146  
 147 Over the last six decades, this region has been studied with multiple approaches, varying  
 148 resolutions, and differing classification methods. Therefore, to provide continuity  
 149 between our analysis and prior work on final glacial-ice occupation and post-glacial  
 150 landscape evolution in the Puget Lowland, we provide a summary of stratigraphic units  
 151 thought to record pre-LGM, LGM, and post-LGM deglaciation and landscape evolution  
 152 in supplement text (Test S1).  
 153

## 154 **2 Materials and Methods**

### 155 **2.1 Sedimentology and stratigraphy**

156 Samples were collected from Whidbey Island outcrops a) Double Bluff, b) Fort  
157 Casey, c) Penn Cove, d) West Beach, and e) Cliffside at 10-cm intervals (Figure 1B;  
158 Table S1) with additional subsamples collected from units with laminations, lenses, or  
159 rip-up clasts. Thin ( $\sim <0.5$ cm thick) horizontally continuous layers are referred to as  
160 laminations, while less continuous layers that pinch out are referred to as a lens (e.g.,  
161 Figure S1). Over 300 discrete bulk sediment samples were analyzed at the University of  
162 Virginia for grain size and magnetic susceptibility (MS). An additional 15 peat, wood,  
163 and marine shell samples were excavated for radiocarbon dating. Grain size analyses  
164 were conducted via a BetterSize S3 Plus Particle analyzer on sample matrix material  
165 (material  $\leq 3$  mm) and MS measurements were collected with a Bartington MS2  
166 magnetic susceptibility meter. MS values provide information about amount and size of  
167 magnetic grains in each sample, elucidating continuity and source of biogenic and  
168 lithogenic deposits (Thompson and Oldfield, 1986; Verosub and Roberts, 1995;  
169 Rosenbaum, 2005; Hatfield et al., 2017; Reilly et al., 2019). Results of the Whidbey  
170 Island stratigraphy are presented according to latitudinal location, starting with the  
171 southernmost site, Double Bluff, followed by the Fort Casey Sites, Penn Cove, West  
172 Beach sites, and ending with the northernmost Cliffside and Rocky Point sites.

### 174 **2.2 Accelerator Mass Spectrometry radiocarbon analysis**

175 Assuming a constant cosmically produced  $^{14}\text{C}$  to  $^{12}\text{C}$  ratio, the variation in this  
176 ratio can be used to determine the amount of time since the death of formerly living  
177 specimens. Samples were run at the National Oceanographic Sciences Accelerator Mass  
178 Spectrometry (NOSAMS) Laboratory at Woods Hole Oceanographic Institute. The  
179 unprocessed wood material underwent a series of six to eight acid-base-acid leaches to  
180 remove contamination and inorganic carbon prior to combustion. The carbonate shell  
181 samples underwent carbonate hydrolysis and resulting carbon combustion reacted with Fe  
182 catalyst along vacuum-sealed lines to produce graphite (Goehring et al., 2019). Resulting  
183 graphite pellets were pressed into targets and analyzed by accelerator mass spectrometry  
184 in addition to standard and processing blanks (Roberts et al., 2019). The AMS  
185 measurements determined the ratio of  $^{14}\text{C}$  to  $^{12}\text{C}$  in each of the pellets, which was then  
186 used to calculate the radiocarbon age using the Libby  $^{14}\text{C}$  half-life of 5,568 years (Stuiver  
187 and Polach, 1977; Stuiver, 1980).

188 Conversion of radiocarbon years to calendar years BP was conducted using the  
189 Int20 curve for terrestrial carbon samples and the Marine20 curve for marine shell  
190 samples using the Calib 8.2 interface (Heaton et al., 2020). Marine20 is the baseline  
191 marine curve used for Calib 8.2 and is the most up-to-date, internationally agreed marine  
192 radiocarbon age calibration curve for non-polar global-average marine records (Heaton et  
193 al., 2020). A marine reservoir correction was calculated in Calib 8.2 and applied to all

194 carbonate shell samples using contemporary shells with known pre-1955 (i.e., prior to  
 195 nuclear bomb testing) collected dates from the Burke Museum in Seattle, Washington.  
 196 The modern (pre-1955) shells from the Burke Institute range in beach-front collection  
 197 date from 1911 to 1931 (Table 1) and include species *Modiolus rectus*, *Musculus niger*,  
 198 *Cardita ventricas*, *Macoma carlottensis*, *Mya arenaria*, and *Macoma nasuta*. The  
 199 radiocarbon ages calculated from these specimens range from  $815 \pm 15$  to  $925 \pm 20$   $^{14}\text{C}$   
 200 years. Utilizing the marine reservoir correction curve developed by Calib 8.2, an average  
 201 marine reservoir correction for this region is  $264$   $^{14}\text{C}$  years (50 calendar years BP). While  
 202 there is a narrow range of marine reservoir effects between 211 and 318  $^{14}\text{C}$  years, a  
 203 species-specific effect was not observed (Table 1).

204  
 205  
 206

**Table 1.** Radiocarbon sample descriptions and data. Gray rows indicate known-age shells dated to develop MRC.

| Name                         | Type       | Age $\pm$ error (RCY) | MRC          | $\Delta 13\text{C}$ | Age $\pm$ error (cal year BP) | actual age (cal year BP) | NOSAMS Receipt # | NOSAMS Accession # |
|------------------------------|------------|-----------------------|--------------|---------------------|-------------------------------|--------------------------|------------------|--------------------|
| WB S1 RCD1 s.h. base U6      | Mollusc    | 1290 $\pm$ 20         | 278 $\pm$ 35 | -0.84               | 1494 $\pm$ 137                | n/a                      | 176236           | OS-164669          |
| WB S1 RCD1 s.h. base U6 clam | Mollusc    | 1210 $\pm$ 25         | 278 $\pm$ 35 | -1.4                | 1563 $\pm$ 130                | n/a                      | 176237           | OS-164670          |
| WB S1 U6 RCD2                | Mollusc    | 1450 $\pm$ 15         | 236 $\pm$ 30 | 0.12                | 1336 $\pm$ 112                | n/a                      | 176238           | OS-164671          |
| PC S3 U3 RCD3                | Mollusc    | 13200 $\pm$ 75        | 278 $\pm$ 35 | 0.44                | 12646 $\pm$ 371               | n/a                      | 176239           | OS-164691          |
| PC S3 U4 RCD5                | Mollusc    | 13000 $\pm$ 75        | 271 $\pm$ 35 | -0.31               | 12305 $\pm$ 327               | n/a                      | 176240           | OS-164692          |
| PC S3 U4 RCD1 a.s.           | Mollusc    | 13250 $\pm$ 75        | 264 $\pm$ 36 | 0.13                | 12749 $\pm$ 366               | n/a                      | 176241           | OS-164693          |
| PC S4 U6 RCD1                | Mollusc    | 1400 $\pm$ 20         | 264 $\pm$ 36 |                     | 1390 $\pm$ 114                | n/a                      | 171379           | OS-160221          |
| PC S3-4 RCD2                 | Mollusc    | 12900 $\pm$ 55        | 264 $\pm$ 36 |                     | 12147 $\pm$ 293               | n/a                      | 171380           | OS-160222          |
| PC S3 RCD4                   | Mollusc    | 13200 $\pm$ 55        | 264 $\pm$ 36 |                     | 12674 $\pm$ 334               | n/a                      | 171381           | OS-160223          |
| PC S3 U4 RCD3                | Mollusc    | 13300 $\pm$ 75        | 216 $\pm$ 30 | 0.33                | 12923 $\pm$ 343               | n/a                      | 176242           | OS-164694          |
| WB S2 U1 RCD1                | Plant/Wood | > 48000               |              | -23.48              |                               | n/a                      | 176243           | OS-164850          |
| PC S4 U6 RCD2                | Mollusc    | 1720 $\pm$ 15         | 236 $\pm$ 30 | -0.06               | 1087 $\pm$ 145                | n/a                      | 176244           | OS-164695          |
| DB S3 RCD1 U4                | Plant/Wood | > 46700               |              |                     |                               | n/a                      | 171378           | OS-160371          |
| DB S5 RCD1 U7                | Plant/Wood | > 48000               |              | -28.62              |                               | n/a                      | 176245           | OS-164851          |
| Mo. r. 6298-1                | Mollusc    | 840 $\pm$ 15          | 236 $\pm$ 30 | 0.15                | 1872 $\pm$ 145                | 91                       | 176246           | OS-164743          |
| Mu. n. 3320-1                | Mollusc    | 860 $\pm$ 25          | 253 $\pm$ 51 | 1.36                | 1860 $\pm$ 148                | 110                      | 176247           | OS-164744          |
| Mu. n. 3320-2                | Mollusc    | 925 $\pm$ 20          | 318 $\pm$ 40 | 1.42                | 1866 $\pm$ 145                | 110                      | 176248           | OS-164745          |
| Ca. v. 13329-1               | Mollusc    | 875 $\pm$ 20          | 270 $\pm$ 40 | 0.49                | 1867 $\pm$ 145                | 104                      | 176249           | OS-164746          |
| Ca. v. 13329-2               | Mollusc    | 890 $\pm$ 15          | 285 $\pm$ 30 | 1.74                | 1871 $\pm$ 144                | 104                      | 176250           | OS-164747          |
| Ma. c. 3348-1                | Mollusc    | 895 $\pm$ 15          | 288 $\pm$ 30 | 0.85                | 1870 $\pm$ 143                | 110                      | 176251           | OS-164748          |
| Ma. c. 3348-2                | Mollusc    | 890 $\pm$ 20          | 283 $\pm$ 40 | 0.05                | 1866 $\pm$ 145                | 110                      | 176252           | OS-164749          |
| My. a. 3427-1                | Mollusc    | 905 $\pm$ 15          | 298 $\pm$ 30 | 0.83                | 1870 $\pm$ 143                | 110                      | 176253           | OS-164750          |
| My. a. 3427-2                | Mollusc    | 850 $\pm$ 20          | 243 $\pm$ 40 | 0.74                | 1866 $\pm$ 145                | 110                      | 176254           | OS-164751          |
| Ma. n. 3470-1                | Mollusc    | 825 $\pm$ 15          | 221 $\pm$ 30 | 0.99                | 1872 $\pm$ 175                | 91                       | 176255           | OS-164760          |
| Ma. n. 3470-2                | Mollusc    | 815 $\pm$ 15          | 211 $\pm$ 30 | 0.39                | 1872 $\pm$ 175                | 91                       | 176256           | OS-164761          |

207  
 208

### 2.3 Optically stimulated luminescence

209 In depositional environments, minerals are exposed to radiation from in situ  
 210 uranium (Ur), thorium (Th), and potassium (K) and cosmic rays (Rhodes, 2011; Duller,  
 211 2015). Incoming radiation excites electrons which are trapped in structure deformities of  
 212 quartz and feldspar grains (Rhodes, 2011). When exposed to sunlight, electrons are  
 213 released from the traps. In returning to their original states, they emit luminescence and  
 214 the mineral is reset. Upon burial, trapped electrons re-accumulate, and the amount is  
 215 proportional to the burial time and the radiation exposure, termed “dose”. The rate of  
 216 irradiation, the “dose rate,” can be calculated from the cosmic flux as well as the U, Th,  
 217 and  $^{40}\text{K}$  concentrations of the surrounding materials. The OSL signal is proportional to  
 218 the dose and can be measured by exposing the mineral to light in a controlled setting. An  
 219 age since burial can be determined by dividing the dose by the dose rate.

220  
 221 Materials from glacial environments present challenges due to the potential of the  
 222 OSL signal not being fully reset between transport and deposition (Wallinga and  
 223 Cunningham, 2015). Additionally, extensive overburden pressure from glacial ice has the

224 potential to partially or completely reset OSL signatures, which could provide large error  
225 to the final OSL stage (King et al., 2014). Subglacial environments, especially those  
226 under ice streams, have a presence of significant meltwater which can saturate sediment  
227 pore space and influence quartz and feldspar exposure to radiation at the time of and for  
228 an extended period of time after deposition (Wallinga and Cunningham, 2015; Duller,  
229 2013).

230 While a detailed description of the OSL procedure can be found in supplement  
231 text (Text S2), a summary is provided here. In order to avoid pre-mature bleaching of  
232 samples, they were collected before sunrise or after sunset, only exposed to low energy  
233 red light, and wrapped in dark black plastic before being transported to East Carolina  
234 University (ECU) for preparation and processing. Samples were prepared for OSL  
235 analysis under dark-room conditions using standard procedures to extract 63-212  $\mu\text{m}$   
236 quartz. Due to feldspar contamination, a post-IR blue SAR procedure was used to  
237 measure the quartz equivalent dose (Murray and Wintle, 2000; Wallinga et al., 2002;  
238 Wintle and Murray, 2006).

239 Bulk sediment was collected from outcrops for high-resolution gamma  
240 spectrometry measurements and stored for at least 4 weeks prior to measurement. OSL  
241 samples were taken at unit boundaries, while dose rate samples were only taken from the  
242 same unit as the OSL samples. Therefore, the gamma dose rates reflect the sample unit  
243 only and contain no information about adjacent, underlying, or overlying units. Uranium  
244 concentrations determined from  $^{234}\text{Th}$  were all significantly higher than concentrations  
245 determined from  $^{214}\text{Pb}$  and  $^{214}\text{Bi}$ . We assumed that  $^{234}\text{U}$  was leached out of the sample  
246 due to in situ water presence.

247 The sample ages, calculated in calendar years, were calculated by dividing the  
248 dose by the dose-rate (Table S2). For samples with feldspar contamination that showed  
249 fading, the ages were corrected as suggested by Auclair et al., (2003). While  $^{14}\text{C}$  ages are  
250 reported in kilo years ago (kya) calendar year BP (1955), all OSL ages are reported in  
251 kya based on the date of collection (2020). OSL ages in kya can be directly compared to  
252 kya cal. BP by subtracting 72 years from the OSL age.

253  
254 **Table 2.** Dose measurements, dose rate, and OSL age data. Final sample ages are bolded.  
255 To directly compare OSL and  $^{14}\text{C}$  ages, it would be necessary to subtract 72 years from  
256 the OSL ages. This correction is considerably smaller than the uncertainty of the ages and  
257 can therefore be neglected.

| Sample    | grain sizes measured | Dose (Gy) | Dose err (Gy) | fading rate (g) (%/decade) | g err | Gamma dose rate (Gy/ka) | Gamma dose rate error | Beta dose rate (Gy/ka) | Beta dose rate error (Gy/ka) | Internal Beta dose rate (Gy/ka) | internal Beta dose rate error (Gy/ka) | total dose rate (Gy/ka) | total dose rate error (Gy/ka) | Age unfaded (ka) | err  | Age after fading (ka) | err |
|-----------|----------------------|-----------|---------------|----------------------------|-------|-------------------------|-----------------------|------------------------|------------------------------|---------------------------------|---------------------------------------|-------------------------|-------------------------------|------------------|------|-----------------------|-----|
| FCS1-OSL1 | 90-125               | 12.13     | 2.82          | 7.1                        | 6.1   | 0.33                    | 0.03                  | 0.61                   | 0.03                         | 0.18                            | 0.07                                  | 1.30                    | 0.09                          | 9.3              | 2.3  | minimum age           |     |
| FCS1-OSL2 |                      |           |               |                            |       |                         |                       |                        |                              |                                 |                                       |                         |                               |                  |      |                       |     |
| FCS2-OSL1 | 63-90                | 92.96     | 7.27          | 3.6                        | 3.8   | 0.67                    | 0.07                  | 1.27                   | 0.06                         | 0.14                            | 0.06                                  | 2.26                    | 0.11                          | 41.2             | 3.8  | 57                    | 16  |
| FCS2-OSL2 | 63-90                | 69.16     | 4.6           | 2.7                        | 2.5   | 0.60                    | 0.06                  | 1.21                   | 0.06                         | 0.14                            | 0.06                                  | 2.13                    | 0.10                          | 32.5             | 2.7  | 40.8                  | 8.2 |
| WBS1-OSL1 | 150-250              | 7.5       | 0.68          | 2.6                        | 5.5   | 0.55                    | 0.06                  | 1.10                   | 0.06                         | 0.36                            | 0.21                                  | 2.20                    | 0.22                          | 3.40             | 0.46 | 4.1                   | 1.8 |
| WBS1-OSL2 | 90-150               | 11.86     | 0.68          | 0                          |       | 0.56                    | 0.07                  | 1.14                   | 0.06                         | 0.00                            | 0.11                                  | 1.90                    | 0.14                          | 6.24             | 0.59 |                       |     |
| WBS2-OSL1 | 90-212               | 64.58     | 4.66          | 3.74                       | 2.5   | 0.67                    | 0.05                  | 1.39                   | 0.06                         | 0.25                            | 0.23                                  | 2.37                    | 0.24                          | 27.2             | 3.4  | 38.1                  | 9.7 |
| WBS2-OSL2 | 90-150               | 70.97     | 4.1           | 0                          |       | 0.67                    | 0.05                  | 1.33                   | 0.07                         | 0.22                            | 0.11                                  | 2.27                    | 0.14                          | 31.3             | 2.7  |                       |     |
| WBS3-OSL1 | 150-212              | 68.43     | 4.96          | 0                          |       | 0.62                    | 0.05                  | 1.20                   | 0.05                         | 0.34                            | 0.04                                  | 2.23                    | 0.08                          | 30.7             | 2.5  |                       |     |
| WBS3-OSL2 | 150-212              | 55.9      | 4.77          | 2.99                       | 1.7   | 0.73                    | 0.06                  | 1.42                   | 0.06                         | 0.25                            | 0.07                                  | 2.47                    | 0.11                          | 22.6             | 2.2  | 29.2                  | 4.6 |
| PCS2-OSL1 | 125-150              | 75.47     | 5.77          | 4.54                       | 0.28  | 0.49                    | 0.04                  | 0.97                   | 0.04                         | 0.45                            | 0.07                                  | 2.05                    | 0.10                          | 36.8             | 3.3  | 56.6                  | 4.1 |
| PCS2-OSL2 | 125-150              | 93.2      | 4.11          | 0                          |       | 0.50                    | 0.04                  | 1.02                   | 0.05                         | 0.45                            | 0.07                                  | 2.10                    | 0.10                          | 44.4             | 2.8  |                       |     |

258

259

### 3 Results

260

We will be moving through results from the southern-most to the northern-most site.

261

Numerical schemes to describe units at each site are independent and do not correlate

262

between sites. Stratigraphic columns were developed to represent our interpretation of

263

physical data present at several locations across these sites and may not reflect all

264

possible interpretations that have been conducted across Whidbey Island.

265

266

#### 3.1 Double Bluff

267

The stratigraphically lower-most unit visible at Double Bluff, Unit 4, is a visually well-sorted sand with sparse rounded gravel lenses. Unit 4 is normally graded with clasts ranging from granule to pebbles with a consistent horizontal long-axis orientation and occasional silt rip-ups from non-visible underlying units. A gradational boundary leads into the overlying sandy silt and fine clayey silt of Unit 3. This unit contains wavy laminations and woody debris dated to be 46.7+ thousand years (kya) cal. BP (i.e., “radiocarbon dead”; Table 1 NOSAMS Receipt #171378). Unit 3 generally fines upwards but with variable matrix grain size modes from 10-500  $\mu\text{m}$  (Figure 1A). Unit 2 is composed of massive diamicton with a clay and fine-silt matrix, marked by a matrix grain size mode of 8  $\mu\text{m}$  and a mix of angular and rounded granule to cobble-sized clasts without a preferred long-axis orientation. There is a gradational contact between Unit 2 and Unit 1. Unit 1 consists of diamicton with a matrix varying between sandy silt and silty sand with woody debris dated to 48.0+ kya cal. BP in age (i.e., “radiocarbon dead”; Table 1 NOSAMS Receipt #176245) and clasts that are predominantly aligned parallel to bedding and evidence of soft-sediment deformation. This uppermost unit has interbedded silt and clay, as well as marine shells in the upper 50 cm of silt that were inaccessible for sampling. MS values in Unit 3 are distinctly lower than the other units (Figure 1A).

284

285

#### 3.2 Fort Casey

286

The lower-most visible unit, Unit 3, at Fort Casey Site 1 consists of massive

287

diamicton with a fine-silt and clay matrix and randomly oriented pebble to cobble-sized

288 angular and rounded clasts. Interbedded with the massive diamicton are discrete gravel  
289 and sand laminations at the base of Unit 3 and silt and clay laminations with rip ups and  
290 woody debris toward the top of Unit 3. Unit 2 consists of fine sand to pebble-size clasts  
291 in a sandy silt matrix with vertically oriented and reverse-graded angular clasts. Unit 2  
292 has a remarkably consistent matrix grain size throughout the unit and a minimum OSL  
293 age of  $9.33 \pm 2.3$  kya (Table 2 Sample #1) from the upper unit boundary (Figure 1A).  
294 This unit also contains sand and silt lenses with mud and plant rip ups (Figure 1A). A  
295 gradational boundary leads to Unit 1, which is massive diamicton similar to Unit 3 but  
296 with a matrix distinctly lighter in color.

297 At Fort Casey Site 2, the lower visible unit, Unit 5, contains interbedded clay and  
298 sand with reverse grading (Figure 1A). Unit 4, in which no samples were collected,  
299 consists of diamicton with concentrated granule to pebble lenses and clay and silt lenses,  
300 as well as evidence of soft-sediment deformation. Unit 3 is a massive clay, followed by  
301 the Unit 2 layer of silt about 20 cm thick, continuous across an irregular, undulating, and  
302 most likely erosional contact. OSL dates at the top of Unit 2 and base of Unit 1 were  
303 found to be  $40.8 \pm 8.2$  and  $56.6 \pm 15.5$  kya (Table 2 Samples #3, 2). The overlying Unit 1  
304 is a diamicton with very fine sand to cobble sized angular and rounded clasts. Normal  
305 grading is present in the matrix of Unit 1 with fractured (i.e., seemingly crushed) granite  
306 clasts.

307

### 308 **3.3 Penn Cove**

309 The lowest visible unit at this site, Unit 5, comprises a reverse-graded diamicton  
310 with a coarsening upward sand matrix and rounded granules and pebbles (Figure 1A).  
311 Following a sharp boundary with Unit 5, Unit 4 consists of silt and sand laminations with  
312 cross-bedded sands near the top. Unit 4 deposits were OSL dated to ages  $56.6 \pm 4.1$  and  
313  $44.4 \pm 2.8$  kya (Table 2 Samples #10, 11). The grain size modes for Unit 4 matrix are  
314 predominantly between 500-700  $\mu\text{m}$  (Figure 1A). An erosional boundary at the top of  
315 Unit 4 leads to the massive clayey silt diamicton of Unit 3 with rounded fine- to cobble-  
316 size clasts and occasional sandy silt and silt lenses. A gradational boundary separates  
317 Units 3 and 2, which is a massive clay diamicton with rounded fine sand to cobble grains  
318 and articulated shells. Six shells from Unit 2 were radiocarbon dated with ages spanning  
319  $12.9 \pm 0.3$  to  $12.1 \pm 0.3$  kya cal. BP (Table 1 NOSAMS Receipt #176239-176242,  
320 171380, 171381). Unit 2 also contains sand lenses and wood fragments. Unit 2 has a  
321 sharp contact with Unit 1, which consists of normally graded gravel with rounded and  
322 angular small to large pebbles with no predominant long-axis orientation. A mode of  
323 clay-sized grains is visible in Units 2 and 3 but is not visible in Unit 1 (Figure 1A).

324

### 325 **3.4 West Beach**

326 At West Beach Site 1, the lowest unit, Unit 5, consists of matrix-supported  
327 diamicton with randomly orientated clasts and two matrix grain size modes at 8 and 20

328  $\mu\text{m}$  (Figure 1A). This unit has a sandy-silt lamination that interrupts the diamicton. The  
329 diamicton above the silty-sand lamination, however, contains highly irregular dips and  
330 soft-sediment deformation. Unit 5 has a gradational boundary with Unit 4 – a light clay  
331 layer deposited on a laterally irregular surface, marked by normal-grading, or fining  
332 upward (Figure 1A). Unit 3 consists of a thick, 0.25-m clast-supported gravel layer with  
333 poorly sorted fine sand to cobble size clasts. A sharp, horizontally regular contact occurs  
334 between Unit 3 to the 0.75 m-thick, well-sorted sand of Unit 2 with OSL ages of  $6.2 \pm 0.6$   
335 and  $4.1 \pm 1.8$  kya (Table 2 Samples #5, 4). Unit 2 has a gradational contact with Unit 1,  
336 which is a modern soil on top of a basal shell hash dating between  $1.56 \pm 0.1$  and  $1.34 \pm$   
337  $0.1$  kya cal. BP (Table 1 NOSAMS Receipt #173237, 176236). MS values are similar  
338 throughout Units 5, 4, 2, and 1, but decrease in Unit 3 (Figure 1A).

339 At the base of West Beach Site 2 are cross-bedded and coarse sand laminations.  
340 OSL dates from the lowermost sand in Unit 8 are dated to  $31.3 \pm 2.7$  and  $38.1 \pm 9.7$  kya  
341 (Table 2 Sample #7, 6). A gradational contact leads into Unit 7, consisting of silt and clay  
342 with radiocarbon-dead woody debris. Unit 6 consists of sand with wavy bedding and silt  
343 laminations. No samples were collected from Units 5 and 4, consisting of a peat layer and  
344 a unit of sand and silt laminations, respectively. The Unit 3 diamicton matrix coarsens  
345 upwards and this unit has many grain size modes between 5 and 70  $\mu\text{m}$  (Figure 1A). Unit  
346 2 consists of diamicton with a fine sand matrix and clasts as large as pebbles and is not  
347 spatially continuous throughout the site. A gradational boundary leads into the 0.5 m-  
348 thick layer of Unit 1, consisting of predominantly of silt.

349

### 350 **3.5 Rocky Point, Cliffside**

351 The lowest visible unit at Cliffside, Unit 6, consists of fine sand to cobble-sized  
352 rounded clasts. This massive diamicton has no preferential orientation for clast long axes.  
353 The matrix changes from clay to sand and includes sediment deformation beneath clasts  
354 (Figure 1A). Unit 6 gradationally transitions to Unit 5, which is a normally graded, fine  
355 sand to cobble-size clast diamicton. Unit 5 is normally graded gravel lenses containing  
356 clasts with consistent horizontal long-axis orientation. Unit 5 gradually transitions into  
357 the granule and sand layer of Unit 4, which includes sand and silt lenses within gravel-  
358 rich and wavy laminations. Unit 3 intrudes into Unit 4 and consists of a massive  
359 diamicton with rounded, cobble-sized clasts. The matrix of Unit 3 has two grain size  
360 modes at 5 and 20  $\mu\text{m}$  (Figure 1A). Two of the lower-unit samples for Cliffside Unit 3  
361 were taken from the more southern Rocky Point site as the identified Unit 3 is continuous  
362 throughout both sites. Unit 3 gradually transitions into Unit 2, which is a laterally  
363 discontinuous light clay unit with silt layers. Unit 1 is comprised of mostly rounded,  
364 normally graded crushed material with fine to large cobble size clasts.

365

### 366 **4 Discussion and Interpretation**

367 We use the sedimentological units described in Section 3 to establish a facies model that  
368 encompasses glaciomarine and coastal sedimentary processes and depositional  
369 environments (i.e., emergent or submergent landscape). Aided by geochronological  
370 constraints, this facies model is applied to the stratigraphic sequences observed at each  
371 site to construct a regional history of ice behavior and landscape evolution before, during,  
372 and following the LGM (Figure 2).

373

#### 374 **4.1 Facies interpretation**

375 Structureless diamicton with randomly oriented clasts of variable size, roundness,  
376 lithology, and a range in matrix size are classified as **glacial till**, or sediments deposited  
377 directly by glaciers in the subglacial environment (Boulton and Deynoux, 1981;  
378 Sengupta, 2017). Some biological material may be incorporated into glacial till in the  
379 form of broken shells or woody fragments. This reworked biogenic material may be  
380 incorporated into the ice as it moves across the landscape, therefore radiocarbon ages of  
381 biogenic material will be older than glacial occupation. These characteristics are  
382 consistent with glaciomarine tills described offshore of West Antarctica (e.g., Kirschner  
383 et al., 2012; Prothro et al., 2018; Smith et al., 2019) and western Greenland (Sheldon et  
384 al., 2016; O'Regan et al., 2021), as well as glacial tills deposited by the relict British-Irish  
385 Ice Sheet (Evans and Thompson, 2010). Lower boundaries of glacial till units are often  
386 characterized by erosional contacts, reflecting glacial advance and erosion of pre-existing  
387 substrate, and may contain rip-up clasts from underlying units. Due to similarities in  
388 structure to formerly identified glacial tills, units classified as (local) LGM glacial till  
389 (i.e., Vashon Till) in the Puget Lowland include Unit 2 from Double Bluff, Unit 3 at Fort  
390 Casey Site 1, Unit 1 from Fort Casey Site 2, Unit 3 from Penn Cove, Unit 5 from West  
391 Beach Site 1, and Unit 6 from Cliffside (Figures 1, 2). Little post-depositional erosion or  
392 reworking of this glacial material is consistent with previous work identifying glacial tills  
393 in the region (Booth & Hallet, 1993; Kovanen & Slaymaker, 2004; Eyles et al., 2018;  
394 Demet et al., 2019).

395 **Glacial outwash** is characterized as diamicton with a range of well-rounded and  
396 some angular clasts with parallel-to-bedding clast orientation that suggests sediment  
397 transport via proglacial meltwater from an upstream source of glacial ice (Boulton and  
398 Deynoux, 1981). This facies may indicate deposition in a subaerial or subaqueous  
399 environment, but importantly, clast orientation distinguishes proglacial outwash from  
400 subglacial till (Boulton and Deynoux, 1981). The deposits may also exhibit normal  
401 grading and/or sedimentary structures indicative of soft-sediment deformation (e.g.,  
402 loading structures, flame structures, sediment deformation beneath clasts; Boulton and  
403 Deynoux, 1981). Glacial outwash recorded in British Columbia (Clague, 1975) and the  
404 forefield of Mýrdalsjökull ice cap in Iceland (Kjær et al., 2004) feature similar structures  
405 seen in several units among our Puget Lowland outcrop sites. Using the defined  
406 classification of glacial outwash, Units 1 and 2 from Fort Casey Site 1, Units 4 and 5

407 from Fort Casey Site 2, Units 1 and 5 from Penn Cove, and Units 1 and 3 from Cliffside  
408 are interpreted as glacial outwash deposits (Figures 1, 2).

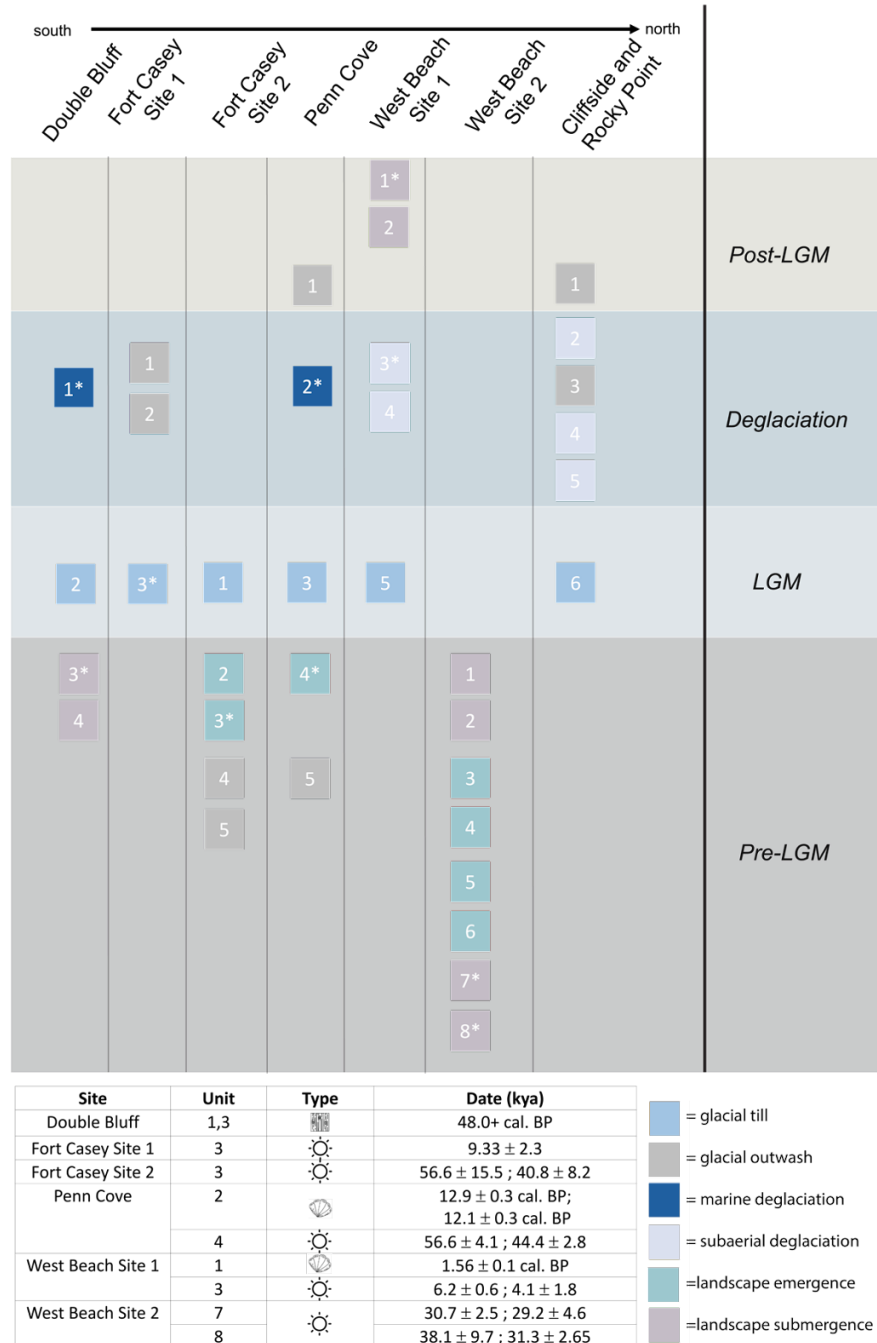
409 A third diamicton, structurally similar to those interpreted as glacial till yet  
410 containing articulated and/or broken marine shells, occasional winnowing of fine-matrix  
411 material, and sedimentary structures such as wavy laminations, is interpreted as  
412 **glacimarine deposits**, composed of both glacial and pelagic sediments that accumulate  
413 on the ocean floor seaward of the ice margin. Such pelagic sediments have been samples  
414 from a geographically-diverse population of sediment cores from deglaciated continental  
415 margins (e.g., Anderson et al., 1980; Prothro et al., 2018; Smith et al., 2019), although  
416 preservation of shells and other carbonate-based materials are less common in Antarctic  
417 glaciomarine sediments. Glacimarine deposits are also identified in coastal outcrop  
418 deposits of northern Svalbard with similar characteristics (Alexanderson et al., 2018).  
419 Both Unit 1 from Double Bluff and Unit 2 from Penn Cove are consistent with these  
420 classifications and closely resemble the structure and composition of the glacimarine  
421 deposits identified on deglaciated continental margins (Figures 1, 2; Anderson et al.,  
422 1980; Prothro et al., 2018). At sites Double Bluff and Penn Cove, this facies (a.k.a.  
423 Everson Glaciomarine Drift) overlays glacial till, indicating ice marginal retreat into a  
424 marine setting with sand-rich deposits recording removal of fines by bottom currents.  
425 Conversely, glacial till that stratigraphically transitions upsection into cross-bedded sands  
426 with parallel-to-bed oriented clasts and wavy laminations that are barren of marine shells  
427 indicate retreat into a subaerial environment, as is observed proximal to the  
428 Mýrdalsjökull ice cap in Iceland (Kjær et al., 2004). Unit 3 from West Beach Site 1 and  
429 Unit 5 from Cliffside record such evidence of **subaerial glacial retreat** both meet these  
430 classifications (Figures 1, 2).

431 Facies transitions where grain sizes coarsen-upward (a.k.a. reverse grading) and  
432 changes in MS values can be associated with **landscape emergence** and differentiation of  
433 source material, respectively (Komar, 1977; McCabe, 1986; Sengupta, 2017). Regardless  
434 of the process(es) explaining the observed grain coarsening, which may include relative  
435 sea level fall outpacing eustatic sea-level rise, tectonic activity, glacial isostatic response,  
436 or a combination of these factors, we would expect such processes to be marked by facies  
437 transitions along the coast. In the Puget Lowland, emergence above sea level has been  
438 recorded in the stratigraphy by thin subaerial deposits (e.g., fluvial sediments and soil)  
439 overlying the glacial and glaciomarine deposits (Domack, 1984; Demet et al., 2019). The  
440 preservation of the glacial till organization and sedimentary structures including cross-  
441 bedding features in the Puget Lowland indicate coarsening-upward seen in the  
442 sedimentary record is not a result of tectonic activity. Coarsening-upward grain sizes seen  
443 in the transition from finer marine sediments to coastal deposits have been identified in  
444 coastal outcrops in northern Svalbard and are interpreted to indicate relative sea level fall  
445 (McCabe, 1986; Alexanderson et al., 2018). While glacial isostatic rebound is not  
446 responsible for the shallowing-upward of Svalbard facies (Alexanderson et al., 2018), the

447 facies and coarsening material identified between Units 3 and 2 at Fort Casey Site 2,  
448 transition from Unit 5 laminated silt to Unit 4 cross-bedded sand at Penn Cove, and  
449 coarsening of grain size with peaks and MS across Units 7 and 6 at West Beach Site 2  
450 could be connected to land emergence events (Figures 1, 2).

451 Facies transitions where grain-sizes fine upward, correspond with increases or  
452 decreases in MS, and are accompanied by the appearance of marine shells are associated  
453 with **landscape submergence** (Sengupta, 2017; Komar, 1977). Similarly classified facies  
454 that mark the transition from a subaerial to a submarine environment have been seen in  
455 seismic profiles and regional stratigraphic data in the southwestern Pacific in South  
456 Island, New Zealand (Carter et al., 1986). Therefore, the fining of material between Unit  
457 4 sand deposits to Unit 3 silts at Double Bluff, introduction of shells to the fining material  
458 between Units 2 and 1 at West Beach Site 1, and fining of grain size across the Unit 2 and  
459 1 boundary at West Beach Site 2 are all interpreted as a transition to a submarine setting  
460 (Figures 1, 2).

461



462

463

**Figure 2.** Grouping of facies based on depositional time periods across Whidbey Island. Units with asterisks have radiocarbon or OSL dates included in the table on the lower left.

464

465

#### 4.2 Pre-LGM landscape evolution

466

467

468

469

470

Prior to glacial advance of the Puget Lobe across Whidbey Island during the LGM, several submergence and emergence facies transitions record dynamic landscape changes. Landscape emergence above sea level prior to LGM glaciation is recorded by outcrops exposed at Penn Cove and Fort Casey Site 2. Penn Cove OSL ages identify this

471 landscape emergence to occur between  $56.6 \pm 4.1$  and  $44.4 \pm 2.8$  kya. Similar Fort Casey  
472 Site 2 OSL ages constrain this transition to having occurred from  $56.6 \pm 15.5$  to  $40.8 \pm$   
473  $8.2$  kya, placing the emergence within the MIS 4 glacial and MIS 3 interglacial stages,  
474 which may be connected to a lack of ice coverage and reduced CIS loading of the solid  
475 Earth at these times.

476 A sequence of submergent and emergent facies are observed in the pre-LGM  
477 deposits at West Beach Site 2. OSL dates places a submergence event between  $38.1 \pm 9.7$   
478 and  $31.3 \pm 2.65$  kya while OSL dates from overlying facies places subsequent emergence  
479 between  $30.7 \pm 2.5$  and  $29.2 \pm 4.6$  kya. Both of these events occurred within the MIS 3  
480 interglacial. This rapid transition between landscape submergence and emergence not  
481 only identifies high sedimentation rates at this site during MIS 3, but also suggests that  
482 the Puget Lowland experienced rapid landscape changes during MIS 3. Clay and sand  
483 deposits included as part of the emergence and submergence interpretation may have  
484 previously been identified and referred to as the Lawton Clay (Mullineaux et al., 1965)  
485 and Esperance Sands, respectively. Prior to LGM ice advance into the Strait of Juan de  
486 Fuca, the Puget Lowland was cut-off and developed into a proglacial lake basin,  
487 responsible for the deposition of the Lawton Clay (Mullineaux et al., 1965). Southward  
488 migrating proglacial channels deposited the Esperance Sands and developed into a large  
489 outwash plain across the Puget Lowland, radiocarbon dated to 18,000-20,000 years ago  
490 (Mullineaux et al., 1965; Crandell et al., 1966; Easterbrook, 1969; Clague, 1976; Booth,  
491 1994). While the uncertainties in our OSL-dates contribute to discrepancy with  
492 previously collected radiocarbon dates of the Esperance Sands (Text S2; Easterbrook,  
493 1969), the OSL ages relative to each other are useful in considering rates of sediment  
494 deposition and landscape evolution.

495

### 496 **4.3 LGM glacial advance**

497 Erosional contacts between glacial till (Vashon Till) and underlying facies mark LGM  
498 advance of the Puget Lobe into the region at multiple sites across Whidbey Island  
499 including Double Bluff, Fort Casey Site 2, and Penn Cove (Figure S2A). OSL ages from  
500 below the erosional contact of LGM tills places maximum age of ice extent at  $56.6 \pm 4.1$   
501 and  $44.4 \pm 2.8$  kya, within the timeframe of MIS 5. However, previously radiocarbon  
502 dated-wood material more precisely dates final LGM advance into the region after 17,500  
503 cal. yr. BP (Mullineaux et al., 1965; Porter & Swanson, 1998; Table 2). This major  
504 difference in ages suggests a great deal of glacial erosion at the ice-bed boundary of the  
505 Puget Lobe during ice advance.

506

### 507 **4.4 Deglaciation**

508 Glacimarine sediments (Everson Glaciomarine Drift) in the uppermost 50 cm of Double  
509 Bluff Unit 1 record retreat of the Puget Lobe within a marine environment (Figure S2B;  
510 Thorson, 1980; Dethier et al., 1995; Demet et al., 2019). At Penn Cove, the presence of

511 articulated shells and winnowing of smaller grain sizes from glacial tills suggests ice  
512 retreat in a marine environment. Five articulated shells found at Penn Cove were  
513 radiocarbon dated to a range of dates between  $12.9 \pm 0.3$  and  $12.1 \pm 0.3$  kya cal. yr. BP  
514 (Table 1), placing glacial ice in this region for ~3,000 years longer than previously  
515 thought (e.g., Easterbrook, 1992; Dethier et al., 1995; Swanson & Caffee, 2001). Based  
516 on the range in shell radiocarbon dates, glacial ice also appears to have been stable at  
517 Penn Cove for at least 1,000 years (Figure 1A) with high sedimentation rates,  
518 accumulating 2.5 m during glaciation. Improved constraints on timing of Puget Lobe  
519 retreat has important implications for eustatic sea-level rise during the late Pleistocene  
520 and suggests Puget Lobe contributions to Meltwater Pulse 1A (Peltier, 2005; Gomez et  
521 al., 2015; Gorbarenko et al., 2019; Yokoyama & Purcell, 2021).

522 Deglacial facies seen at the more northern West Beach Site 1 and Cliffside  
523 indicate ice retreat within a subaerial environment (Figure S2A). The change in ice retreat  
524 style seen from the more southern Double Bluff and Penn Cove sites to the northern West  
525 Beach and Cliffside sites may be due to the substantial, 1,000-year stand-still of ice at  
526 Penn Cove. The duration of ice stability at this location is an indication that ice retreat  
527 was step-wise, rather than catastrophic (c.f., Easterbrook, 1992). Step-wise retreat of the  
528 ice margin is also supported by the presence of grounding-zone wedges (GZWs); the  
529 development of these ice-marginal landforms were likely supported by the identified high  
530 rates of sedimentation in the region (~2.5 mm/year; Simkins et al., 2017; Simkins et al.,  
531 2018; Demet et al., 2019). Additionally, the Rocky Point site features a bedrock high  
532 (i.e., a potential pinning point of ice; Hogan et al., 2020) and mapped GZWs, suggesting  
533 this site could have periodically stabilized ice during land rebound before final  
534 deglaciation of the region (Simkins et al., 2018; Demet et al., 2019).

535

#### 536 **4.5 Post-LGM landscape evolution**

537 Following deglaciation of Whidbey Island, the Penn Cove and Cliffside sites  
538 record outwash deposits from proglacial fluvial sources. An OSL age within the  
539 submergence facies of Unit 2 at West Beach Site 1 marks the transition from a post-  
540 glacial fluvial environment to a submarine environment between  $6.2 \pm 0.6$  and  $4.1 \pm 1.8$   
541 kya. Radiocarbon-dated shell hash sampled from the uppermost unit at this same West  
542 Beach Site 1 suggests a highly energetic aquatic marine or coastal environment was  
543 present in this location as early as  $1.56 \pm 0.1$  kya cal. BP, at least 5,000 years following  
544 ice loss in the Puget Lowland. After initial lithospheric rebound from ice-loading and the  
545 possibility of a local tectonic event, it is feasible vertical land movement slowed enough  
546 to allow local sea level to resubmerge the region around 1,000 years ago (Figure 1A, 2).  
547 Overall, findings from this work support better understanding of the extinct CIS while  
548 also elucidating the role GIA and subglacial topography may play in determining ice-  
549 margin retreat styles for systems with similar subglacial topography and rheologic

550 settings such as margins of Greenland and the Antarctic Peninsula (Eyles et al., 2018;  
551 Whitehouse et al., 2019; Nield et al., 2014).

552

## 553 **5 Conclusions**

554 This decimeter-scale physical sedimentological assessment, paired with  
555 geochronological assessment of seven sites across the deglaciated Puget Lowland,  
556 provides spatiotemporal information on landscape emergence and submergence as well as  
557 final ice advance and retreat of the southernmost CIS. Rates of vertical landscape changes  
558 constrained through OSL dating indicates the Puget Lowland was a highly dynamic  
559 region where a sequence of landscape emergence and submergence occurred within  
560 ~1,000 years during MIS 3 despite the concurrent period of rapid and substantial global  
561 mean sea level rise (Yokoyama & Purcell, 2021). Additionally, these findings place  
562 glacial ice in the Puget Lowland for 3,000 years longer during the LGM than previously  
563 thought, with final retreat occurring across the middle of Whidbey Island at  
564 approximately  $12.1 \pm 0.3$  kya cal. BP, which may have implications for contributions to  
565 Meltwater Pulse 1A. Radiocarbon dates are used to show ice marginal stand-still and  
566 substantial grounding zone sedimentation during final retreat. While more southern sites  
567 (e.g., Double Bluff and Penn Cove) record ice retreat within submarine environments, the  
568 northernmost sites (e.g., Cliffside and Rocky Point), which feature a topographic high  
569 and previously mapped grounding-zone wedges (Demet et al., 2019), appear to record ice  
570 retreat into a subaerial environment. This data records empirical evidence of rapid  
571 vertical landscape evolution and paired marine-terminating ice stability for at least a  
572 millennium. The similarities between the rheology in this location and the rheology of the  
573 Antarctic Peninsula, as well as the topographic similarities between the Puget Lowland  
574 and modern margins of the Greenland Ice Sheet make these findings highly relevant to  
575 increasing process-based understanding of solid Earth influence on ice dynamics in  
576 contemporary marine-terminating glacial systems.

## 577 **Acknowledgments**

578 The sites analyzed for this work are located on land historically cultivated and inhabited by the  
579 Skokomish, Suquamish, Squaxin, Stl'pulmsh, Steilacoom, Puyallup, Muckleshoot, and  
580 Duwamish peoples, while much of the data analysis and interpretation were conducted on land  
581 cultivated and inhabited by the Monacan Nation. The peoples of these Nations were custodians of  
582 the land for time immemorial before forced removal and genocide during colonization. The  
583 authors acknowledge their ongoing stewardship of the lands. This work was funded by the  
584 Chamberlain Endowment and the H.G. Goodell Endowment at the University of Virginia. The  
585 funding and support for the radiocarbon dates presented was made possible through the  
586 NOSAMS Graduate Student Internship at Woods Hole Institute, supported by NSF cooperative  
587 agreement OCE-1755125, and the Burke Institute. Thank you to Dr. Mark Kurz, Dr. Roberta  
588 Hansman, Anne Cruz, Mary Lardie Gaylord, and Nan Trowbridge for their hospitality and  
589 guidance throughout M. McKenzie's internship. The authors declare that they have no conflict of  
590 interest.

591

## 592 **Open Research**

593 Digital data including site coordinates and sample grain size, trace element (not included in  
594 analysis), moisture content, and magnetic susceptibility data and all 236 physical samples are  
595 housed in the PANGAEA database (McKenzie et al., *submitted*) and at the Washington  
596 Department of Natural Resources at the Washington Geological Survey. Physical samples are in  
597 WhirlPak bags, labelled by site name, number, and sampling interval in centimeters. When  
598 collected in the field, unit names were given from down-to-up outcrop. For the purpose of  
599 simplicity, the unit names were flipped for manuscript analyses to be listed as smallest to highest  
600 up-to-down outcrop. To request physical data, please contact Jessica Czajkowski  
601 ([Jessica.Czajkowski@dnr.wa.gov](mailto:Jessica.Czajkowski@dnr.wa.gov)) and/or Ashley Cabibbo ([Ashley.Cabibbo@dnr.wa.gov](mailto:Ashley.Cabibbo@dnr.wa.gov)) at the  
602 Washington State Department of Natural Resources.

603

## 604 **References**

- 605 Alexanderson, H., Henriksen, M., Ryen, H.T., Landvik, J.Y., & Peterson, G. (2018). 200 ka of  
606 glacial events in NW Svalbard: an emergence cycle facies model and regional correlations.  
607 *Arktos*, 4, 1-25. <https://doi.org/10.1007/s41063-018-0037-z>
- 608 Alley, R. B., Holschuh, N., MacAyeal, D. R., Parizek, B. R., Zoet, L., Riverman, K., Muto, A.,  
609 Christianson, K., Clyne, E., Anandakrishnan, S., Stevens, N., & GHOST Collaboration.  
610 (2021). Bedforms of Thwaites Glacier, West Antarctica: Character and Origin. *Journal of*  
611 *Geophysical Research: Earth Surface*, 126(12). <https://doi.org/10.1029/2021JF006339>
- 612 Anderson, J.B., Kurtz, D.D., Domack, E.W., & Balshaw, K.M. (1980). Glacial and Glacial  
613 Marine Sediments of the Antarctic Continental Shelf. *The Journal of Geology*. 88(4).  
614 <https://www.journals.uchicago.edu/doi/pdf/10.1086/628524>
- 615 Anundsen, K., Abella, S., Leopold, E., Stuiver, M., & Turner, S. (1994). Late-Glacial and Early  
616 Holocene Sea-Level Fluctuations in the Central Puget Lowland, Washington, Inferred from  
617 Lake Sediments. *Quaternary Research*, 42(2), 149–161.  
618 <https://doi.org/10.1006/qres.1994.1064>
- 619 Armstrong, J.E., Crandell, D.R., Easterbrook, D.J., & Noble, J.B. (1965). Late  
620 Pleistocene Stratigraphy and Chronology in Southwestern British Columbia and  
621 Northwestern Washington. *Geological Society of America*, 76(3), 321-330.
- 622 Auclair, M., Lamothe, M., & Huot, S. (2003). Measurement of anomalous fading for feldspar  
623 IRSL using SAR. *Radiation Measurements*, 37(4), 487–492. [https://doi.org/10.1016/S1350-4487\(03\)00018-0](https://doi.org/10.1016/S1350-4487(03)00018-0)
- 625 Barbouti, A. I., & Rastin, B. C. (1983). A study of the absolute intensity of muons at sea level and  
626 under various thicknesses of absorber. *Journal of Physics G: Nuclear Physics*, 9(12), 1577.  
627 <https://doi.org/10.1088/0305-4616/9/12/018>
- 628 Booth, D. B. (1987). Timing and processes of deglaciation along the southern margin of the  
629 Cordilleran ice sheet. In W. F. Ruddiman & H. E. Wright (Eds.), *North America and Adjacent*  
630 *Oceans During the Last Deglaciation* (pp. 71–90). Geological Society of America.  
631 <https://doi.org/10.1130/DNAG-GNA-K3.71>
- 632 Booth, D. B., & Hallet, B. (1993). Channel networks carved by subglacial water: Observations  
633 and reconstruction in the eastern Puget Lowland of Washington. *Geological Society of*  
634 *America Bulletin*, 105(5), 671–683. [https://doi.org/10.1130/0016-7606\(1993\)105<0671:CNCBSW>2.3.CO;2](https://doi.org/10.1130/0016-7606(1993)105<0671:CNCBSW>2.3.CO;2)
- 636 Booth, D. (1994). Glaciofluvial infilling and scour of the Puget Lowland, Washington, during ice  
637 sheet glaciation. *Geology*, 22, 695-698.

638 Booth, D. B., Troost, K. G., Clague, J. J., & Waitt, R. B. (2003). The Cordilleran Ice Sheet. In  
639 *Developments in Quaternary Sciences* (Vol. 1, pp. 17–43). Elsevier.  
640 [https://doi.org/10.1016/S1571-0866\(03\)01002-9](https://doi.org/10.1016/S1571-0866(03)01002-9)

641 Bøtter-Jensen, L., & Murray, A. S. (1999). Developments in Optically Stimulated Luminescence  
642 Techniques for Dating and Retrospective Dosimetry. *Radiation Protection Dosimetry*, 84(1),  
643 307–315. <https://doi.org/10.1093/oxfordjournals.rpd.a032745>

644 Boulton, G. S., & Deynoux, M. (1981). Sedimentation in glacial environments and the  
645 identification of tills and tillites in ancient sedimentary sequences. *Precambrian Research*,  
646 15(3–4), 397–422. [https://doi.org/10.1016/0301-9268\(81\)90059-0](https://doi.org/10.1016/0301-9268(81)90059-0)

647 Carter, R.M., Carter, L., & Johnson, D.P. (1986). Submergent shorelines in the SW Pacific:  
648 evidence for an episodic post-glacial transgression. *Sedimentology*, 33(5), 629–649.  
649 <https://doi.org/10.1111/j.1365-3091.1986.tb01967.x>

650 Clague, J. J. (1975). Sedimentology and paleohydrology of late Wisconsinan outwash, Rocky  
651 Mountain trench, southeastern British Columbia. *Glaciofluvial and Glaciolacustrine*  
652 *Sedimentation*.

653 Clague, J.J. (1976). Quadra Sand and its relation to the late Wisconsin glaciation of  
654 southwest British Columbia. *Canadian Journal of Earth Sciences*, 13(6), 717–875.

655 Clague, J. J. (1981). Late Quaternary geology and geochronology of British Columbia, Part  
656 2. Geological Survey of Canada, 80-35, 41.

657 Clark, P. U. (1994). Unstable Behavior of the Laurentide Ice Sheet over Deforming Sediment and  
658 Its Implications for Climate Change. *Quaternary Research*, 41(1), 19–25.  
659 <https://doi.org/10.1006/qres.1994.1002>

660 Clarke, G. K. C., Nitsan, U., & Paterson, W. S. B. (1977). Strain heating and creep instability in  
661 glaciers and ice sheets. *Reviews of Geophysics*, 15(2), 235.  
662 <https://doi.org/10.1029/RG015i002p00235>

663 Crandell, D.R., Mullineaux, D.R., & Waldron, H.H. (1966). Age and origin of the Puget  
664 Sound trough in western Washington. U.S. Geological Survey, 525-B, B132-B136.

665 Cuffey, K., & Paterson, W. S. B. (2010). *The physics of glaciers* (4th ed). Butterworth-  
666 Heinemann/Elsevier.

667 Demet, B. P., Nittrouer, J. A., Anderson, J. B., & Simkins, L. M. (2019). Sedimentary processes  
668 at ice sheet grounding-zone wedges revealed by outcrops, Washington State (USA). *Earth*  
669 *Surface Processes and Landforms*, 44(6), 1209–1220. <https://doi.org/10.1002/esp.4550>

670 Dethier, D. P., Pessl, F., Keuler, R. F., Balzarini, M. A., & Pevear, D. R. (1995). Late  
671 Wisconsinan glaciomarine deposition and isostatic rebound, northern Puget Lowland,  
672 Washington. *Geological Society of America Bulletin*, 107(11), 1288–1303.  
673 [https://doi.org/10.1130/0016-7606\(1995\)107<1288:LWGDAI>2.3.CO;2](https://doi.org/10.1130/0016-7606(1995)107<1288:LWGDAI>2.3.CO;2)

674 Domack, E.W. (1984). Rhythmically Bedded Glaciomarine Sediments on Whidbey Island,  
675 Washington. *SEPM Journal of Sedimentary Research*, Vol. 54.  
676 <https://doi.org/10.1306/212F847C-2B24-11D7-8648000102C1865D>

677 Domack, E.W. (1983). Facies of late Pleistocene glacial-marine sediments on Whidbey  
678 Island, Washington: An isostatic glacial-marine sequence in Molnia, B.F. (ed.) *Glacial-*  
679 *Marine Sedimentation*: Plenum, New York, 535–570.

680 Duller G.A.T. (2013). *Luminescence Analyst*, 4.11 ed, Aberystwyth University.

681 Duller, G.A.T. (2015). Luminescence dating. In W.J. Rink, & J.W. Thompson (Eds.),  
682 *Encyclopedia of Scientific Dating Methods* (pp. 390–404). (Encyclopedia of Earth Science  
683 Series). Springer Nature.

684 Durand, G., Gagliardini, O., Favier, L., Zwinger, T., & Le Meur, E. (2011). Impact of bedrock  
685 description on modeling ice sheet dynamics: BEDROCK DESCRIPTION TO MODEL  
686 ICE SHEET. *Geophysical Research Letters*, 38(20), n/a-n/a.

687 Easterbrook, D. J. (1992). Advance and Retreat of Cordilleran Ice Sheets in Washington, U.S.A.  
688 *Géographie Physique et Quaternaire*, 46(1), 51–68. <https://doi.org/10.7202/032888ar>

689 Easterbrook, D.J., Crandell, D.R., & Leopold, E.B. (1967). Pre-Olympia Pleistocene  
690 stratigraphy and chronology in the central Puget Lowland, Washington. *Geological Society of*  
691 *America Bulletin*, 78(1), 13-20.

692 Easterbrook, D. (1969). Pleistocene Chronology of the Puget Lowland and San Juan  
693 Islands, Washington. *Geological Society of America Bulletin*, 80, 2273-2286.

694 Easterbrook, D.J. (1986). Stratigraphy and chronology of Quaternary deposits of the Puget  
695 Lowland and Olympic Mountains of Washington and the Cascade Mountains of  
696 Washington and Oregon. *Quaternary Science Reviews*, 5, 145-159.

697 Evans, D.J.A., & Thompson, S.A. (2010) Glacial sediments and landforms of Holderness, eastern  
698 England: A glacial depositional model for the North Sea Lobe of the British-Irish Ice Sheet.  
699 *Earth-Science Reviews* 101(3-4), p. 147-189. <https://doi.org/10.1016/j.earscirev.2010.04.003>

700 Eyles, N., Arbelaez Moreno, L., & Sookhan, S. (2018). Ice streams of the Late Wisconsin  
701 Cordilleran Ice Sheet in western North America. *Quaternary Science Reviews*, 179, 87–122.  
702 <https://doi.org/10.1016/j.quascirev.2017.10.027>

703 Favier, L., Pattyn, F., Berger, S., & Drews, R. (2016). Dynamic influence of pinning points on  
704 marine ice-sheet stability: a numerical study in Dronning Maud Land, East Antarctica. *The*  
705 *Cryosphere*, 10(6), 2623–2635. <https://doi.org/10.5194/tc-10-2623-2016>

706 Galbraith, R. F., Roberts, R. G., Laslett, G. M., Yoshida, H., & Olley, J. M. (1999). Optical  
707 dating of single and multiple grains of quartz from Jinmium rock shelter, Northern Australia:  
708 Prt 1, Experimental design and statistical models. *Archaeometry*, 41(2), 339–364.  
709 <https://doi.org/10.1111/j.1475-4754.1999.tb00987.x>

710 Goebel, T. Waters, M., & O’rourke, D. (2011). The Late Pleistocene Dispersal of  
711 Modern Humans in the Americas. *Science*, 319, 1497.

712 Goehring, B. M., Wilson, J., & Nichols, K. (2019). A fully automated system for the extraction of  
713 in situ cosmogenic carbon-14 in the Tulane University cosmogenic nuclide laboratory. *Nuclear*  
714 *Instruments and Methods in Physics Research Section B: Beam Interactions with Materials*  
715 *and Atoms*, 455, 284–292. <https://doi.org/10.1016/j.nimb.2019.02.006>

716 Gomez, N., Gregoire, L. J., Mitrovica, J. X., & Payne, A. J. (2015). Laurentide-Cordilleran Ice  
717 Sheet saddle collapse as a contribution to meltwater pulse 1A. *Geophysical Research*  
718 *Letters*, 42(10), 3954-3962. <https://doi.org/10.1002/2015GL063960>

719 Gorbarenko, S., Shi, X., Zou, J., Velivetskaya, T., Artemova, A., Liu, Y., Yanchenko, E. &  
720 Vasilenko, Y. (2019). Evidence of meltwater pulses into the North Pacific over the last 20 ka  
721 due to the decay of Kamchatka Glaciers and Cordilleran Ice Sheet. *Global and Planetary*  
722 *Change*, 172, 33-44. <https://doi.org/10.1016/j.gloplacha.2018.09.014>

723 Guérin, G., Mercier, N., Adamic, G., (2011). Dose-rate conversion factors: update. *Ancient TL*  
724 29(1), 5-8.

725 Hatfield, R. G., Stoner, J. S., Reilly, B. T., Tepley, F. J., Wheeler, B. H., & Housen, B. A. (2017).  
726 Grain size dependent magnetic discrimination of Iceland and South Greenland terrestrial  
727 sediments in the northern North Atlantic sediment record. *Earth and Planetary Science Letters*,  
728 474, 474–489. <https://doi.org/10.1016/j.epsl.2017.06.042>

729 Heaton, T. J., Köhler, P., Butzin, M., Bard, E., Reimer, R. W., Austin, W. E. N., Bronk Ramsey,  
730 C., Grootes, P. M., Hughen, K. A., Kromer, B., Reimer, P. J., Adkins, J., Burke, A., Cook, M.  
731 S., Olsen, J., & Skinner, L. C. (2020). Marine20—The Marine Radiocarbon Age Calibration  
732 Curve (0–55,000 cal BP). *Radiocarbon*, 62(4), 779–820. <https://doi.org/10.1017/RDC.2020.68>

733 Hogan, K.A., Larter, R.D., Graham, A.G.C., Arthern, R., Kirkham, J.D., Totten, R.L., Jordan,  
734 T.A., Clark, R., Fitzgerald, V., Wählín, A.K., Anderson, J.B., Hillenbrand, C., Nitsche, F.O.,  
735 Simkins, L., Smith, J.A., Gohl, K., Arndt, J.E., Hong, J., & Wellner, J. (2020). Revealing the  
736 former bed of Thwaites Glacier using sea-floor bathymetry: implications for warm-water  
737 routing and bed controls on ice flow and buttressing. *The Cryosphere* 14(9), p. 2883-2908.  
738 <https://doi.org/10.5194/tc-14-2883-2020>

739 Jamieson, S. S. R., Vieli, A., Livingstone, S. J., Cofaigh, C. Ó., Stokes, C., Hillenbrand, C.-D., &  
740 Dowdeswell, J. A. (2012). Ice-stream stability on a reverse bed slope. *Nature Geoscience*,  
741 5(11), 799–802. <https://doi.org/10.1038/ngeo1600>

742 King, G. E., Robinson, R. A. J., & Finch, A. A. (2014). Towards successful OSL sampling  
743 strategies in glacial environments: deciphering the influence of depositional processes on  
744 bleaching of modern glacial sediments from Jostedal, Southern Norway. *Quaternary Science  
745 Reviews*, 89, 94–107. <https://doi.org/10.1016/j.quascirev.2014.02.001>

746 Kirshner, A. E., Anderson, J. B., Jakobsson, M., O'Regan, M., Majewski, W., & Nitsche, F. O.  
747 (2012). Post-LGM deglaciation in Pine island Bay, west Antarctica. *Quaternary Science  
748 Reviews*, 38, 11-26. <https://doi.org/10.1016/j.quascirev.2012.01.017>

749 Kjær, K.H., Sultan, L., Krüger, J., & Schomacker, A. (2004). Architecture and sedimentation of  
750 outwash fans in front of the Mýrdalsjökull ice cap, Iceland. *Sedimentary Geology*, 172(1-2),  
751 139-163. <https://doi.org/10.1016/j.sedgeo.2004.08.002>.

752 Komar, P. (1977). BEACH PROCESSES AND SEDIMENTATION. *Beach Processes and  
753 Sedimentation*.

754 Kovanen, D. J., & Slaymaker, O. (2004). Relict Shorelines and Ice Flow Patterns of the Northern  
755 Puget Lowland from Lidar Data and Digital Terrain Modelling. *Geografiska Annaler. Series A,  
756 Physical Geography*, 86(4), 385–400. <https://www.jstor.org/stable/3566155>

757 Leopold, E. B., Nickmann, R., Hedges, J. I., & Ertel, J. R. (1982). Pollen and Lignin Records of  
758 Late Quaternary Vegetation, Lake Washington. *Science*, 218(4579), 1305–1307.  
759 <https://doi.org/10.1126/science.218.4579.1305>

760 Lesnek, A. J., Briner, J. P., Lindqvist, C., Baichtal, J. F., & Heaton, T. H. (2018). Deglaciation of  
761 the Pacific coastal corridor directly preceded the human colonization of the Americas. *Science  
762 Advances*, 4(5), eaar5040. <https://doi.org/10.1126/sciadv.aar5040>

763 Mandryk, C. A. S., Josenhans, H., Fedje, D. W., & Mathewes, R. W. (2001). Late Quaternary  
764 paleoenvironments of Northwestern North America: implications for inland versus coastal  
765 migration routes. *Quaternary Science Reviews*, 20(1), 301–314. [https://doi.org/10.1016/S0277-3791\(00\)00115-3](https://doi.org/10.1016/S0277-3791(00)00115-3)

766

767 Margold, M., Stokes, C. R., & Clark, C. D. (2015). Ice streams in the Laurentide Ice Sheet:  
768 Identification, characteristics and comparison to modern ice sheets. *Earth-Science Reviews*,  
769 143, 117–146. <https://doi.org/10.1016/j.earscirev.2015.01.011>

770 McCabe, A.M. (1986). Glaciomarine facies deposited by retreating tidewater glaciers; an  
771 example from the late Pleistocene of Northern Ireland. *Journal of Sedimentary Research*. 56  
772 (6): 880–894. doi: <https://doi.org/10.1306/212F8A76-2B24-11D7-8648000102C1865D>

773 McKenzie, M. A., Miller, L. E., Lepp, A. P., & DeWitt, R. (submitted) Physical and chemical  
774 sedimentology conducted on coastal outcrops across Whidbey Island, Washington state.  
775 PANGAEA Data Archiving & Publication (PDI-36347).

776 McKenzie, M. A., Miller, L. E., Slawson, J. S., MacKie, E. J., & Wang, S. (2023). Differential  
777 impact of isolated topographic bumps on ice sheet flow and subglacial processes. *The  
778 Cryosphere*, 17(6), 2477-2486. <https://doi.org/10.5194/tc-17-2477-2023>

779 Menounos, B., Goehring, B.M., Osborn, G., Margold, M., Ward, B., Bond, J., ... & Heyman, J.  
780 (2017). Cordilleran Ice Sheet mass loss preceded climate reversals near the Pleistocene  
781 Termination. *Science*, 358(6364), 781-784.

782 Mullineaux, D.R., Waldron, H.H., & Rubin, M. (1965). Stratigraphy and chronology of  
783 late interglacial and early Vashon time in the Seattle area, Washington. U.S. Geological  
784 Survey Bulletin, 1194-O, 10.

785 Murray, A. S., & Wintle, A. G. (2000). Luminescence dating of quartz using an improved single-  
786 aliquot regenerative-dose protocol. *Radiation Measurements*, 32(1), 57–73.  
787 [https://doi.org/10.1016/S1350-4487\(99\)00253-X](https://doi.org/10.1016/S1350-4487(99)00253-X)

788 Nield, G. A., Barletta, V. R., Bordoni, A., King, M. A., Whitehouse, P. L., Clarke, P. J., Domack,  
789 E., Scambos, T. A., & Berthier, E. (2014). Rapid bedrock uplift in the Antarctic Peninsula

790 explained by viscoelastic response to recent ice unloading. *Earth and Planetary Science*  
 791 *Letters*, 397, 32–41. <https://doi.org/10.1016/j.epsl.2014.04.019>  
 792 O'Regan, M., Cronin, T. M., Reilly, B., Alstrup, A. K. O., Gemery, L., Golub, A., ... &  
 793 Jakobsson, M. (2021). The Holocene dynamics of Ryder Glacier and ice tongue in north  
 794 Greenland. *The Cryosphere*, 15(8), 4073-4097. <https://doi.org/10.5194/tc-15-4073-2021>  
 795 Peltier, W.R. (2005). On the hemispheric origins of meltwater pulse 1a. *Quaternary Science*  
 796 *Reviews*. 24(14-15) p. 1655-1671. <https://doi.org/10.1016/j.quascirev.2004.06.023>  
 797 Pessl Jr., F., Dethier, D.P., Keuler, R.F., Minard, J.P., & Balzarini, M.A. (1981).  
 798 Sedimentary facies and depositional environments of late Wisconsin glacial-marine deposits  
 799 in the central Puget Lowland, Washington. American Association Petroleum Geologists,  
 800 Abstracts, Arm. Meeting, San Francisco.  
 801 Polenz, M., Slaughter, S. L., & Thorsen, G. W. (2005). Geologic map of the Coupeville and  
 802 part of the Port Townsend North 7.5-minute quadrangles, Island County,  
 803 Washington. Washington Division of Geology and Earth Resources Geologic Map, GM-58, 1  
 804 sheet, scale 1: 24,000.  
 805 Porter, S. C., & Swanson, T. W. (1998). Radiocarbon Age Constraints on Rates of Advance and  
 806 Retreat of the Puget Lobe of the Cordilleran Ice Sheet during the Last Glaciation. *Quaternary*  
 807 *Research*, 50(3), 205–213. <https://doi.org/10.1006/qres.1998.2004>  
 808 Powell, R.D. (1980). Holocene glacial-marine deposition by tide-water glaciers in Glacier  
 809 Bay, Alaska [unpublished Ph.D. thesis]. Ohio State University.  
 810 Prescott, J. R., Stephan, L. G. (1982). The contribution of cosmic radiation to the environmental  
 811 dose for thermoluminescence dating. *PACT*, 6, 17–25.  
 812 <https://cir.nii.ac.jp/crid/1573668924373277824>  
 813 Prescott, J. R., & Hutton, J. T. (1994). Cosmic ray contributions to dose rates for luminescence  
 814 and ESR dating: Large depths and long-term time variations. *Radiation Measurements*, 23(2),  
 815 497–500. [https://doi.org/10.1016/1350-4487\(94\)90086-8](https://doi.org/10.1016/1350-4487(94)90086-8)  
 816 Prothro, L.O., Simkins, L.M., Majewski, W., & Anderson, J.B. (2018). Glacial retreat  
 817 patterns and processes determined from integrated sedimentology and geomorphology  
 818 records. *Marine Geology*, 395, 104-119.  
 819 Reilly, B. T., Stoner, J. S., Mix, A. C., Walczak, M. H., Jennings, A., Jakobsson, M., Dyke, L.,  
 820 Glueder, A., Nicholls, K., Hogan, K. A., Mayer, L. A., Hatfield, R. G., Albert, S., Marcott, S.,  
 821 Fallon, S., & Cheseby, M. (2019). Holocene break-up and reestablishment of the Petermann  
 822 Ice Tongue, Northwest Greenland. *Quaternary Science Reviews*, 218, 322–342.  
 823 <https://doi.org/10.1016/j.quascirev.2019.06.023>  
 824 Rhodes, E. J. (2011). Optically Stimulated Luminescence Dating of Sediments over the Past  
 825 200,000 Years. *Annual Review of Earth and Planetary Sciences*, 39(1), 461–488.  
 826 <https://doi.org/10.1146/annurev-earth-040610-133425>  
 827 Rigg, G. B., & Gould, H. R. (1957). Age of Glacier Peak eruption and chronology of post-glacial  
 828 peat deposits in Washington and surrounding areas. *American Journal of Science*, 255(5), 341–  
 829 363. <https://doi.org/10.2475/ajs.255.5.341>  
 830 Robel, A. A., Pegler, S. S., Catania, G., Felikson, D., & Simkins, L. M. (2022). Ambiguous  
 831 stability of glaciers at bed peaks. *Journal of Glaciology*, 68(272), 1177–1184.  
 832 <https://doi.org/10.1017/jog.2022.31>  
 833 Roberts, M. L., Elder, K. L., Jenkins, W. J., Gagnon, A. R., Xu, L., Hlavenka, J. D., &  
 834 Longworth, B. E. (2019). <sup>14</sup>C Blank Corrections for 25–100 µg Samples at the National Ocean  
 835 Sciences AMS Laboratory. *Radiocarbon*, 61(5), 1403–1411.  
 836 <https://doi.org/10.1017/RDC.2019.74>  
 837 Rosenbaum, J. G. (2005). Magnetic properties of sediments in cores BL96-1,-2, and-3 from Bear  
 838 Lake, Utah and Idaho. *US Geological Survey Open-File Report*, (1203), 13p.  
 839 Sengupta, S. (2017). *Introduction to Sedimentology* (1st ed.). Routledge.  
 840 <https://doi.org/10.1201/9780203749883>

841 Sheldon, C., Jennings, A., Andrews, J.T., Ó Cofaigh, C., Hogan, K., Dowdeswell, J.A., &  
842 Seidenkrantz, M. (2016). Ice stream retreat following the LGM and onset of the west  
843 Greenland current in Uummannaq Trough, west Greenland. *Quaternary Science Reviews*, 147,  
844 p. 27-46. <https://doi.org/10.1016/j.quascirev.2016.01.019>

845 Sherrod, B. L., Blakely, R. J., Weaver, C. S., Kelsey, H. M., Barnett, E., Liberty, L., Meagher, K.  
846 L., & Pape, K. (2008). Finding concealed active faults: Extending the southern Whidbey Island  
847 fault across the Puget Lowland, Washington. *Journal of Geophysical Research*, 113(B5),  
848 B05313. <https://doi.org/10.1029/2007JB005060>

849 Shugar, D. H., Walker, I. J., Lian, O. B., Eamer, J. B. R., Neudorf, C., McLaren, D., & Fedje, D.  
850 (2014). Post-glacial sea-level change along the Pacific coast of North America. *Quaternary*  
851 *Science Reviews*, 97, 170–192. <https://doi.org/10.1016/j.quascirev.2014.05.022>

852 Simkins, L. M., Anderson, J. B., & Demet, B. P. (2017). Grounding line processes of the southern  
853 Cordilleran Ice Sheet in the Puget Lowland. In R. A. Haugerud & H. M. Kelsey, *From the*  
854 *Puget Lowland to East of the Cascade Range* <sub>title>Geologic Excursions in the Pacific  
855 *Northwest*</sub>. Geological Society of America. [https://doi.org/10.1130/2017.0049\(03\)](https://doi.org/10.1130/2017.0049(03))

856 Simkins, L. M., Greenwood, S. L., & Anderson, J. B. (2018). Diagnosing ice sheet grounding line  
857 stability from landform morphology. *The Cryosphere*, 12(8), 2707–2726.  
858 <https://doi.org/10.5194/tc-12-2707-2018>

859 Smith, J.A., Graham, A.G.C., Post, A.L. Hillenbrand, C., Bart, P. J., & Powell, R.D. (2019). The  
860 marine geological imprint of Antarctic ice shelves. *Nat Commun* 10, 5635 (2019).  
861 <https://doi.org/10.1038/s41467-019-13496-5>

862 Stuiver, M., & Polach, H. A. (1977). Discussion reporting of <sup>14</sup>C data. *Radiocarbon*, 19(3), 355-  
863 363. <https://doi.org/10.1017/S0033822200003672>

864 Stuiver, M. (1980). Workshop On <sup>14</sup>C Data Reporting. *Radiocarbon*, 22(3), 964–966.  
865 <https://doi.org/10.1017/S0033822200010389>

866 Swanson, T. W., & Caffee, M. L. (2001). Determination of <sup>36</sup>Cl Production Rates Derived from  
867 the Well-Dated Deglaciation Surfaces of Whidbey and Fidalgo Islands, Washington.  
868 *Quaternary Research*, 56(3), 366–382. <https://doi.org/10.1006/qres.2001.2278>

869 Thompson, R., & Oldfield, F. (1986). *Environmental Magnetism*. London, Allen & Unwin.

870 Thorson, R. M. (1980). Ice-Sheet Glaciation of the Puget Lowland, Washington, during the  
871 Vashon Stade (Late Pleistocene)1. *Quaternary Research*, 13(3), 303–321.  
872 [https://doi.org/10.1016/0033-5894\(80\)90059-9](https://doi.org/10.1016/0033-5894(80)90059-9)

873 Thorson, R.M. (1981). Isostatic effects of the last glaciation in the Puget lowland,  
874 Washington. U.S. Geological Survey Open-File Report, 81-370, 100.

875 Thorson, R. (1989). Glacio-isostatic response of the Puget Sound area, Washington.  
876 Geological Society of America Bulletin, 101, 1163-1174.

877 van der Wal, W., Whitehouse, P. L., & Schrama, E. J. (2015). Effect of GIA models with 3D  
878 composite mantle viscosity on GRACE mass balance estimates for Antarctica. *Earth and*  
879 *Planetary Science Letters*, 414, 134-143. <https://doi.org/10.1016/j.epsl.2015.01.001>

880 Verosub, K. L., & Roberts, A. P. (1995). Environmental magnetism: Past, present, and future.  
881 *Journal of Geophysical Research: Solid Earth*, 100(B2), 2175–2192.  
882 <https://doi.org/10.1029/94JB02713>

883 Waitt Jr., R.B., & Thorson, R.M. (1983). The Cordilleran ice sheet is Washington, Idaho,  
884 and Montana. Late-quaternary environments of the United State, 1, 53-70.

885 Wallinga, J., & Cunningham, A. C. (2015). Luminescence dating, uncertainties and age range.  
886 *Encyclopedia of Scientific Dating Methods*, 440–445. [https://doi.org/10.1007/978-94-007-](https://doi.org/10.1007/978-94-007-6304-3_197)  
887 [6304-3\\_197](https://doi.org/10.1007/978-94-007-6304-3_197)

888 Wallinga, J., S. Murray, A., & Btter-Jensen, L. (2002). Measurement of the Dose in Quartz in the  
889 Presence of Feldspar Contamination. *Radiation Protection Dosimetry*, 101(1), 367–370.  
890 <https://doi.org/10.1093/oxfordjournals.rpd.a006003>

891 Wan, J. X. W., Gomez, N., Latychev, K., & Han, H. K. (2022). Resolving glacial isostatic  
892 adjustment (GIA) in response to modern and future ice loss at marine grounding lines in West  
893 Antarctica. *The Cryosphere*, 16(6), 2203-2223. <https://doi.org/10.5194/tc-16-2203-2022>  
894 Weertman, J. (1974). Stability of the Junction of an Ice Sheet and an Ice Shelf. *Journal of*  
895 *Glaciology*, 13(67), 3–11. <https://doi.org/10.3189/S0022143000023327>  
896 Whillans, I. M., & Van Der Veen, C. J. (1997). The role of lateral drag in the dynamics of Ice  
897 Stream B, Antarctica. *Journal of Glaciology*, 43(144), 231–237.  
898 <https://doi.org/10.3189/S0022143000003178>  
899 Whitehouse, P. L., Gomez, N., King, M. A., & Wiens, D. A. (2019). Solid Earth change and the  
900 evolution of the Antarctic Ice Sheet. *Nature Communications*, 10(1), 503.  
901 <https://doi.org/10.1038/s41467-018-08068-y>  
902 Whitehouse, P.L. (2018). Glacial isostatic adjustment modelling: historical perspectives, recent  
903 advances, and future directions. *Earth Surface Dynamics*, 6, 401-429.  
904 <https://doi.org/10.5194/esurf-6-401-2018>.  
905 Willis, B. (1898). Drift phenomena of Puget Sound. *Geological Society of America Bulletin*,  
906 9, 111-16  
907 Wintle, A. G., & Murray, A. S. (2006). A review of quartz optically stimulated luminescence  
908 characteristics and their relevance in single-aliquot regeneration dating protocols. *Radiation*  
909 *Measurements*, 41(4), 369–391. <https://doi.org/10.1016/j.radmeas.2005.11.001>  
910 Wintle AG. (1973). Anomalous fading of thermoluminescence in mineral samples. *Nature*  
911 245:143–44  
912 Yokoyama, Y., & Purcell, A. (2021). On the geophysical processes impacting palaeo-sea-level  
913 observations. *Geoscience Letters*, 8(1), 13. <https://doi.org/10.1186/s40562-021-00184-w>  
914